

# Branching and path-deviation of positive streamers resulting from statistical photon transport

Zhongmin Xiong<sup>1</sup> and Mark J Kushner<sup>2</sup>

Electrical Engineering and Computer Science Department, University of Michigan, Ann Arbor, MI 48109-2122, USA

E-mail: [zax@esi-group.com](mailto:zax@esi-group.com), [zxiong@umich.edu](mailto:zxiong@umich.edu) and [mjkush@umich.edu](mailto:mjkush@umich.edu)

Received 28 May 2014, revised 6 September 2014

Accepted for publication 17 September 2014

Published 27 October 2014

## Abstract

The branching and change in direction of propagation (path-deviation) of positive streamers in molecular gases such as air likely require a statistical process which perturbs the head of the streamer and produces an asymmetry in its space charge density. In this paper, the mechanisms for path-deviation and branching of atmospheric pressure positive streamer discharges in dry air are numerically investigated from the viewpoint of statistical photon transport and photoionization. A statistical photon transport model, based on randomly selected emitting angles and mean-free-path for absorption, was developed and embedded into a fluid-based plasma transport model. The hybrid model was applied to simulations of positive streamer coaxial discharges in dry air at atmospheric pressure. The results show that secondary streamers, often spatially isolated, are triggered by the random photoionization and interact with the thin space charge layer (SCL) of the primary streamer. This interaction may be partly responsible for path-deviation and streamer branching. The general process consists of random remote photo-electron production which initiates a back-traveling electron avalanche, collision of this secondary avalanche with the primary streamer and the subsequent perturbation to its SCL. When the SCL is deformed from a symmetric to an asymmetric shape, the streamer can experience an abrupt change in the direction of propagation. If the SCL is sufficiently perturbed and essentially broken, local maxima in the SCL can develop into new streamers, leading to streamer branching. During the propagation of positive streamers, this mechanism can take place repetitively in time and space, thus producing multi-level branching and more than two branches within one level.

Keywords: positive streamer, branching, photon-transport, atmospheric pressure

(Some figures may appear in colour only in the online journal)

## 1. Introduction

Electrical gas discharges at high pressures in molecular gases are often filamentary. In such cases, ionization takes place predominately in the form of streamers or ionization waves and the ionized gas occupies narrow channels trailing behind the streamer heads [1–3]. In an open, atmospheric pressure

environment, the typical plasma channel width is hundreds to thousands of microns, and the propagation speed of the streamer head is on the order of  $10^7$ – $10^9$  cm s<sup>-1</sup> [4–10]. The trajectory of a streamer rarely closely follows the direction of the externally applied electrical field over long distances. Such streamers often have sharp turns (path-deviation) and branches, resulting in a tree-like structure of the plasma channels [6, 11, 12]. While the former represents an abrupt deviation in the direction of propagation, the latter is a topological change in the structure of the streamer. Lightning,

<sup>1</sup> Present address: ESI US R&D, 32605 W 12 Mile Road, Suite 350, Farmington Hills, MI 48334, USA.

<sup>2</sup> Author to whom any correspondence should be addressed.

both below (downward strikes) and above the thunderclouds (e.g. elves, sprites), is an example of naturally occurring streamer discharges whose paths display many deviations and branches [13]. In addition to the interest in fundamental discharge physics, streamer dynamics define plasma intensity and uniformity in many high-pressure, industrial applications. For example, in ozone generation by corona discharges, the same pulse with positive polarity generates twice the amount of ozone as with a negative polarity pulse, an effect in part attributed to the former producing more streamer channels and branches than the latter [14, 15]. On the other hand, pre-ionization is typically needed for gas discharge lasers to suppress the formation of the streamers in order to enhance the plasma uniformity, which is essential to the optical quality of the laser beam [16, 17].

The general dynamics of streamer propagation are well understood. The internal electric field generated by space charge separation in the head of the streamer produces rapid ionization which advances the streamer head [1–3, 18–19]. Negative streamers typically rely on transport of electrons into the non-ionized zone in front of the streamer head to provide seed electrons for the avalanche. Positive streamers typically rely on photoionization to provide these seed electrons [20–24]. The space charge generated electric field is often much stronger than the externally applied electric field and so the details of the space charge field tend to determine the direction and mode of the propagation. However, the detailed mechanism of path-deviation and streamer branching, as an active response to the instantaneous and local environment in front of the streamer head, is not well understood [25–27].

The seemingly random occurrence of path-deviation and streamer branching, both spatially and temporally, suggests a statistical mechanism for seeding electrons immediately ahead of the streamer. This seeding of electrons is a pre-requisite for streamer propagation and particularly so for positive streamers [1–3]. For negative, or anode directed streamers, where the seed electrons are produced predominately by electron transport in the same direction as the streamer propagates, the statistical nature of the electron seeding has found increasing support from advanced experimental diagnostics and sophisticated computer models [28–32]. Many salient features of the negative streamers, such as the channel width, the propagation speed and the electrical structure of streamer head, can largely be captured by using a two-species (one electron and one ion) fluid discharge model [26, 30–32]. It was found that the space charge layer (SCL), which provides the large electric field in the head of the streamer, is typically much thinner than the streamer head radius. These works also found that the stability of the SCL plays an important role in determining the characteristics of the streamers [30–31, 33]. For a negative, planar ionization front, the destabilizing electron impact ionization is balanced by the stabilizing electron transport. A planar ionization front can be destabilized by ripple-type perturbations and eventually develop into a fingering pattern [34].

Despite the promising results by linear stability analysis, computational models based on fully deterministic fluid formulation, have difficulty reproducing a streamer branching

and path-deviation [30–32]. Fully deterministic, three-dimensional (3D) models are capable of predicting branching. For example, Kolobov and Arslanbekov [35] computationally demonstrated the formation of nearly periodic, near anode streamers which propagated in different directions. The small differences in plasma density between these streamers resulted in only a subset surviving far from the anode. This is likely a consequence of the initial triggering of the instability that produces branching, which is also likely to be stochastic in nature, judging by the spontaneous and random appearances of path-deviation and branching. As a result, the instabilities are not well captured in such deterministic fluid models. In purely fluid deterministic models, the seed or triggering electrons in the non-ionized region ahead of the streamer are usually described by a continuous density function resulting from electron drift and diffusion across the negative streamer head. Due to the large density gradient across the thin SCL, the electron density flowing into the neutral region ahead of the streamer head can be rather low. From a simulation standpoint, the product of the density of the seeding electrons ahead of the streamer head times the volume of the computational cell could yield less than 1 electron per numerical cell. In such low density regions, the electron dynamics may be better described by a particle approach. In this vein, computational models based on fluid, hybrid and particle formulations have been developed to investigate the branching of negative streamers [31, 32]. It was found that streamer branching could be predicted by the random electron seeding processes which were enabled by hybrid and fully kinetic models, while fully fluid models do not exhibit such phenomena [32]. These studies demonstrated the importance of the statistical electron seeding on the development of branching in negative streamers.

The instability and branching processes of positive or cathode directed streamers are thought to be more complex than negative or anode directed streamers [36–39]. This is primarily due to photoionization, an intrinsically non-local process, which is a likely source for seed electrons ahead of the streamer and so responsible for the propagation of positive streamers. Unlike its negative counterpart, electron transport in positive streamers generally cannot provide seed electrons ahead of the streamer since they travel in the opposite direction to the streamer propagation. So in the absence of pre-ionization (such as due to previous discharge pulses or radiation from cosmic rays), photon-ionization produced by the streamer itself is likely the prevailing process responsible for producing seed electrons [36]. Simulations suggest that photoionization still dominates the pre-ionization ahead of the streamer in air, unless the level of the pre-ionization is above  $10^{10} \text{ cm}^{-3}$  [37].

Given the importance of pre-ionization to propagation of positive streamers, it is natural to consider its role in path-deviation and branching of positive streamers, and in particular the stochastic manner that photoionization generates seed electrons. The importance of seed ionization in branching has been quantified by Pancheshnyi in 3D simulations in cathode directed streamers [40]. The statistical spatial distribution of low levels of pre-ionization can

initiate branching and other non-uniformities in the streamer structure. Statistical pre-ionization, or stochastic fluctuations, in the propagation streamer ionization fronts have also been numerically addressed by Arrayas *et al* [41]. They found that fluctuations can accelerate ionization fronts compared to the otherwise identical deterministic case.

There is not a readily available linear stability analysis for positive streamers incorporating non-local photoionization to provide insights to their stability. Photoionization being the source of stochastic seed electrons has found certain support in recent studies. For example, experiments of positive streamers in high purity nitrogen have identified feather like structures connected to the main plasma channel. It was hypothesized that these structures are due to individual electron avalanches moving toward the main channel [38]. By introducing electron-density fluctuations into a fluid model, finite perturbations were introduced to the propagation of the streamer head which destabilized the head and could eventually lead to streamer branching in air [39]. We should note, however, that although including a photoionization model in a fluid model enables the propagation of positive streamers, our simulations and those reported in the literature have found that photoionization enhances the stability of streamers rather than destabilizing them [42, 43]. As a result, fluid based computational models with photoionization have not been clearly shown to produce streamer branching or strong path-deviation as observed in experiments [30, 31].

Photoionization of air requires production of VUV radiation by the streamer head from excited states that are produced by electron impact excitation in the tail of the electron energy distribution. The sparse nature of this VUV radiation, coupled with small photoionization cross sections, likely produces a statistical distribution of seed electrons ahead of the streamer head, as opposed to a smooth continuum as would be predicted by conventional radiation transport. The stochastic nature of the seed electrons produced by the photoionization at and in front of the head of a positive streamer has the potential to play an important role in path-deviation and branching. For example, Vereshchagin and Beloglowsky [44] showed that the likelihood for seed ionization ahead of a positive streamer to produce branching depends on the local electric field in which the ionization occurs, and the shielding of the electric field by adjacent branches. To examine these processes, a statistical radiation transport model was embedded into a two-dimensional (2D) fluid plasma transport simulation. In this paper, we discuss results from this model for positive streamer stability, branching and path-deviation. Admittedly, streamer branching and path-deviation are likely 3D phenomena. However, we believe the dominant underlying mechanisms can still be captured by proper 2D (but not axisymmetric) simulations. The photon transport model presented in this paper takes into account the density distributions of the emitting and absorption species, the lifetime of the emitting states and more importantly the non-local and stochastic nature of photon transport and absorption process. This work builds upon prior investigations that have addressed statistical photon transport in the context of streamer propagation by quantifying the role of continuous

or discontinuous space charge layers in path deviation and branching. We used this statistical model to simulate positive streamer discharges in dry air at atmospheric pressure in a coaxial configuration.

The numerical results show that secondary, often spatially isolated, electron avalanches triggered by the random photoionization ahead of the streamer can interact with the thin SCL of the primary streamer. This interaction may be responsible for abrupt path-deviation and branching of the primary streamer. The general dynamical process consists of the random remote photo-electrons initiating a back-traveling electron avalanche which collides with the primary streamer and disrupts the SCL. If the SCL is sufficiently perturbed, the streamer will branch. Otherwise the streamer may abruptly deviate from its original path as the SCL loses its symmetry. As the positive streamer propagates, this mechanism can take place repetitively at random times and spatial locations, producing several levels of branching and sometimes more than two branches in one level.

The statistical photon transport model and comparison with the existing, continuum based radiation transport model are presented in section 2, along with a brief description of the coaxial discharge configuration and the simulation conditions. The numerical results for a positive streamer discharge in dry air at atmospheric pressure are presented in section 3. Our emphasis is on the statistical nature of the photon transport and its effects on the stability and topology of the streamer structures, as well as its connection to the streamer branching and path-deviation. Our discussion and concluding remarks are in section 4.

## 2. Description of the photon transport model

### 2.1. 2D plasma hydrodynamics model with deterministic photon transport

The 2D simulations of positive streamers in dry air at atmospheric pressure were performed using *nonPDPSIM*, a plasma hydrodynamics model with radiation transport [45, 46]. Based on a 2D unstructured, finite volume discretization, *nonPDPSIM* solves the transport equations for all charged species and Poisson's equation for electric potential using a fully implicit Newton's method. Updates of the charged particle densities and electric potential are followed by an implicit update of the electron temperature,  $T_e$ , neutral particle densities, kinetic secondary electron transport and neutral flow field properties. The use of the electron energy equation allows for non-equilibrium between the local electric field and the electron transport coefficients, which are obtained from stationary solutions of Boltzmann's equation.

The existing photon transport model in *nonPDPSIM* is based on a deterministic, Green's function or propagator approach. The photoionization source for species  $m$  at location  $\vec{r}_i$  due to the emission of photons at location  $\vec{r}_j$  by species  $k$  is

$$S_m(\vec{r}_i) = \sigma_{km}^I N_m(\vec{r}_i) A_k \int N_k(\vec{r}_j) G_k(\vec{r}_j, \vec{r}_i) d^3\vec{r}_j \quad (1)$$

$$G_k(\vec{r}_j, \vec{r}_i) = \frac{1}{4\pi |\vec{r}_j - \vec{r}_i|^2} \exp \left[ - \int_{\vec{r}_j}^{\vec{r}_i} \sum_l \sigma_{lk} N_l(\vec{r}_n) d\vec{r}_n \right], \quad (2)$$

where  $N_k$  is the density of the radiating species having the Einstein coefficient  $A_k$ ,  $\sigma_{km}^l$  is the photoionization cross section for species  $m$  by photons emitted by species  $k$ , and  $\sigma_{lk}$  is the total absorption cross section for photon  $k$  by species  $l$ .  $G_k(\vec{r}_j, \vec{r}_i)$  is a Green's function which captures the survival of the photons emitted at the location  $\vec{r}_j$  to reach location  $\vec{r}_i$  and also accounts for view angles, obscurations and the decrease in flux due to isotropic propagation. The density of the emitting state,  $N_k(\vec{r}_j)$  comes from its continuity equation that accounts for formation and quenching processes. We develop the Green's function for every emitting point to every absorbing point by integrating along the trajectory between the two points for the integral within the exponent. This technique was developed to account for conditions where the density of absorbers is a function of position due to chemistry or initial conditions (such as a He jet injected into air). The technique also allows for including obscurations, transmission of radiation through windows and an arbitrary combination of non-ionizing and ionizing radiation. Although the density of absorbers is constant here, there is the matter of obscuration represented by the center electrode. The Green's function can become very large since it accounts for  $N^2/2$  ( $N$  is the number of mesh points) pairwise emission-absorption interactions. In practice, we limit the distance from any given emission point for which the Green's function is computed.

In principle, our deterministic model is the same as that developed by Bourdon *et al* [24] following from the work of Zhelezniak *et al* [22] for photoionization in air. In Bourdon's work, semi-analytic expressions were developed for the propagation kernel, the equivalent of our Green's function, valid over specified ranges of partial pressures of  $O_2$ , and multiple photon groups were employed. The photoionizing source of radiation was expressed as a function of the rate of electron impact excitation of the radiating state, and ratios of rates of quenching to radiative relaxation. The end result is that Bourdon's model is accurate to high order and computationally efficient. In our model, we have included these processes purely numerically in order to account for the discussed spatial dependence of absorbers and obscurations, and to enable a variety of absorbers. Another difference is that we also directly compute the density of the emitting states through their own continuity equations, and so the consequences of quenching are already included in the density of the emitter. The penalty we pay for a more general approach is that the technique is less computationally efficient and more subject to mesh effects.

The use of  $G_k(\vec{r}_j, \vec{r}_i)$  assumes a uniform photon flux propagating outward from the point of emission in a spherically symmetric fashion *at any time instant*, as illustrated in figure 1(a). In reality, given the discrete nature of the photons and the statistical nature of their emission, this mean behavior represented by this continuum approach results from an ensemble average of many discrete events. The spherical shape of the shell of expanding photon flux results from a time averaged photon flux, in which individual photons are emitted

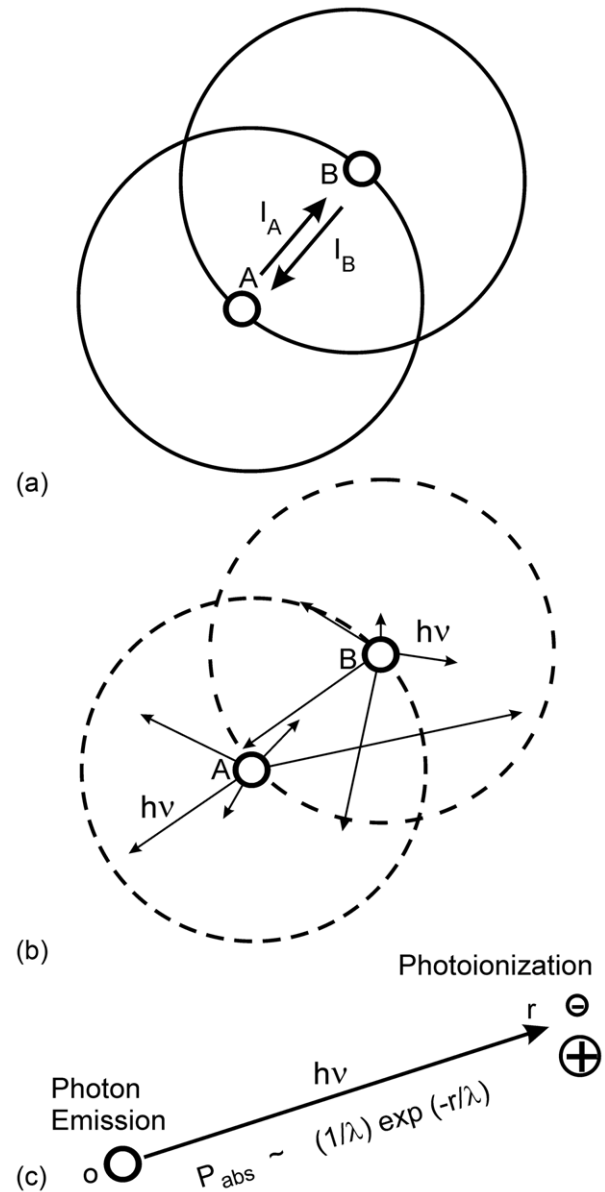


**Figure 1.** Schematics of (a) flux-based, deterministic and (b) particle-type, statistical photon transport models. The probability of photon absorption/ionization (c), with a photon mean free path  $\lambda$ , at a distance  $r$  from the emission site.

with equal probability into any solid angle. The continuum approach also assumes that, given the density of absorbers is constant, the cumulative probability for absorption of the photon flux is isotropic and only a function of radial distance. Again, this is a statically averaged result. In the limit of large numbers of photons, this mean photon flux approach works well. However, even starting with large number photons, the natural decrease in the photon flux resulting from the spherical expansion, and further reductions by absorption, will eventually result in there being a statistically small number of photons at the expanding radiation front.

There is also a numerical consideration that may bring into question continuum photon emission for such conditions. The number of photons emitted from a numerical cell having volume  $V$  during integration timestep  $\Delta t$  for an excited state

density  $N$  and radiative lifetime  $\tau$  is  $n = NV\Delta t/\tau$ . The size of the numerical cell in simulations of streamers may be a small as  $10\text{--}20\ \mu\text{m}$  and the integration time steps  $< 10^{-11}\ \text{s}$ , while excited state densities are  $10^{12}\text{--}10^{13}\ \text{cm}^{-3}$  and lifetime of high lying excited states is  $5\text{--}10\ \text{ns}$ . The end result is that only a few photons, on the average, may be emitted from a numerical cell during an integration time step.

As the photon flux decreases (or if it is initially small) there may be large fluctuations in the instantaneous photon fluxes and the distances at which they get absorbed. For example, in the continuum model, a location closer to the emission point will always receive a larger photon flux than a point at a further distance. However this is only true in an ensemble average but not instantaneously. Although a fully deterministic model, as described above, is adequate in modeling the time and spatially averaged property of photon transport, it is not the optimum model to investigate conditions where statistical fluctuations of photon transport, photon absorption and ionization may play a dominate role, such as in the branching and path-deviation of streamers. In such cases, the dynamics of the streamer discharge depend on the local and instantaneous environment that the streamer heads encounter, rather than an ensemble averaged environment.

## 2.2. Statistical photon transport model

Photon transport within a plasma media is an intrinsically stochastic process. The time at which photons are emitted after the creation of the excited state is randomly described by Poisson statistics with mean lifetime  $A^{-1}$ , where  $A$  is the Einstein coefficient. Although not addressed in this study, photons are randomly emitted in frequency across their spectral line-shape function. These photons are emitted in a random direction. Their mean free path before absorption is probabilistic, also typically Poisson distributed with a mean free path given by  $(\sigma N)^{-1}$ , where  $\sigma$  is the absorption cross section and  $N$  is the density of the absorbing species.

We have developed a simple statistical photon transport model which uses a particle-like approach, rather than a deterministic propagator, to treat photon transport in plasmas. The model relaxes the constraint of instantaneous spherical symmetry of photon transport, but statistically recovers the distribution on an ensemble averaged basis. The continuum photon transport in the present mode is approximated by a large number of the macro-photon particles as illustrated schematically in figure 1(b), each having a random propagation angle and random absorption distance (based on appropriate probability distribution), whose collective behavior represents the averaged photon transport property expressed in equation (2). Specifically, the implementation of the statistics photo transport model consists of the following steps.

- 1 In space, the neighboring domain of an emission point  $i$  at  $\vec{r}_i$  is divided into a total number of  $N$  elements or subdomains having volume  $V_k$ . Each sub-domain contains a variable number of numerical grid points. For example in the 2D case, one can divide the neighboring region into  $N = N_\theta N_r$  domains with  $N_\theta$  and  $N_r$  being the number of divisions in the azimuthal and radial directions.

In the 3D case,  $N_\theta$  should uniformly partition the solid angle of  $4\pi$ . The summation of the mesh points contained within the  $V_k$  sub-volumes for a given emission point represents all possible locations where photons emitted from this point can be absorbed. This distribution of mesh points needs to be computed only once in the code.

- 2 At a time  $t$ , the instantaneous number of photons,  $N_p$ , emitted from each emission point within a small time interval is computed. The time interval  $dt \ll \tau_r$ , where  $\tau_r$  is the radiative lifetime of the state. The number of photons emitted from the cell is  $N_p = N_e V_e A dt$ , where  $N_e$  is the density of the emitting state,  $A$  is its Einstein coefficient and  $V_e$  is the volume of the emitting cell.
- 3 The number of actual photons per photon pseudoparticle,  $n_p$ , is chosen.
- 4 A random number  $r_\theta$  uniformly distributed between  $[0,1]$  is chosen to determine the solid angle into which the  $n_p$  photons will be emitted.
- 5 A random number  $r_r$  uniformly distributed between  $[0,1]$  is chosen to determine the distance from the emission point where the  $n_p$  photons will be absorbed, as shown figure 1(c). The probability distribution for absorption for a distance  $r$  is

$$P(r) = \frac{1}{\lambda} \exp\left(\frac{-r}{\lambda}\right), \quad \lambda = \left(\sum_k \sigma_k N_k\right)^{-1}, \quad (3)$$

where  $\lambda$  is the mean free path for absorption,  $N_k$  is the density of the absorbing species having absorption cross section  $\sigma_k$ .

- 6 A search is made to locate the sub-volume corresponding to the randomly chosen angle and absorption distance. In that sub-volume, there are  $N_m$  mesh points.
- 7 A test is made to determine if the absorption produces a photoionization. If

$$r \leq f_I, \quad f_I = \frac{\sigma_I N_I}{\sum_k \sigma_k N_k} \quad (4)$$

then an ionization occurs. Here,  $f_I$  is the fraction of absorptions producing ionization,  $r$  is a random number  $[0,1]$ ,  $N_I$  is the density of the photoionized absorbing species having photoionization cross section  $\sigma_I$ . If an ionization does not occur, then one proceeds to the emission of the next photon pseudoparticle.

- 8 An ionization rate ( $\text{cm}^3\text{s}^{-1}$ ) is then computed for each mesh point in the sub-volume  $k$ , in which the photoionization occurs. The change in electron density,  $n_e$ , is

$$\frac{dn_e}{dt} = \frac{n_p f_I}{V_k N_e dt}. \quad (5)$$

This ionization rate is then added to the rate equations for electrons, ionization neutral and ion.

- 9 Repeat from step 3  $N_p/n_p$  times for each emitting point or until all photons are emitted.
- 10 Repeat from step 2 for all the emission points in the plasma.
- 11 Repeat from step 2 at the next time instant  $t + dt$ .

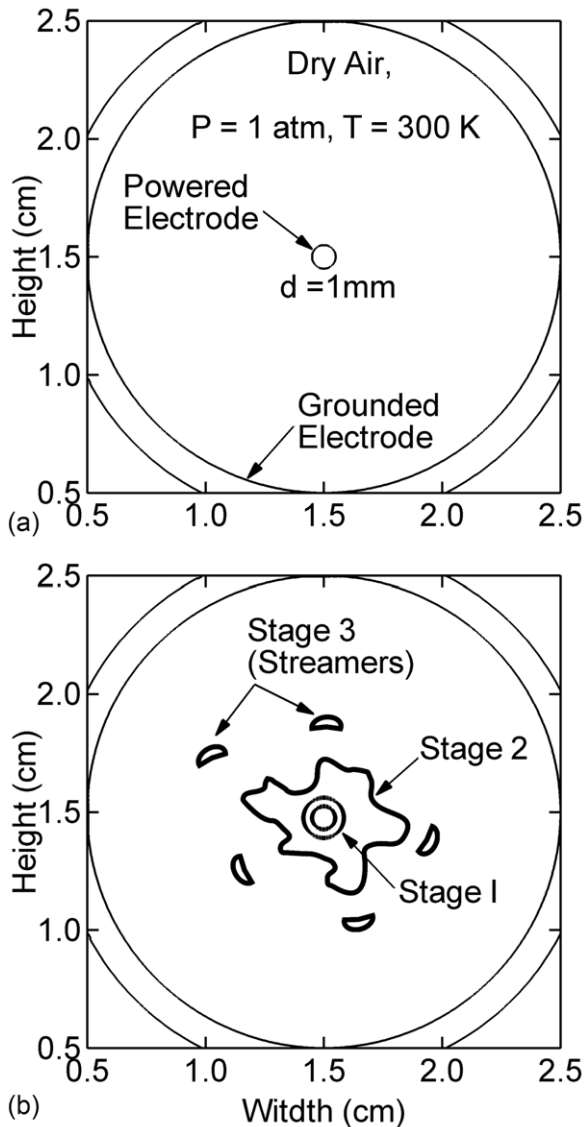


**Figure 2.** Discharge configuration for positive streamers in dry air at atmospheric-pressure. (a) Coaxial geometry. The diameters of the inner powered electrode and the grounded outer electrode are 1 and 20 mm. A positive, 14 ns dc voltage pulse of 50 kV with 1 ns rise and fall times is applied to the powered electrode. (b) Schematic of the 3 stages for individual streamers emerging from a destabilized ionization front. The initially circular ionization front (stage 1) is destabilized and produces vestiges of individual streamers (stage 2). The individual streamers (stage 3) emerge by breaking away from distorted ionization front.

The number of the emitted photons per time step,  $N_P$ , at from each emitting point should be much smaller than the total number of photons emitted from the emitting sub-volume by all excited states during a radiative lifetime. At the same time,  $N_P$  should also be large enough to avoid too small a time step  $dt$ . We found by experience that  $dt \approx (10^{-3} - 10^{-4})/A$  is a good compromise.

### 2.3. Discharge configuration and modeling conditions

A coaxial, annular discharge, shown in figure 2(a), was used to investigate photon transport and the propagation of positive

streamers. This coaxial configuration is similar to that used in the experiments described by Wang *et al* [47] however in these computations the discharge is only 1/4 of its size. This choice was made so that our numerical mesh could be fine enough to minimize numerical effects. The outer (hollow) cylinder is the grounded electrode and has an inner diameter of 2 cm while the center (solid) rod serves as the powered electrode with a 1 mm diameter. The entire computational domain (not shown) is a square region with a side length of 3 cm. The annular space between the electrodes is filled with dry air ( $N_2 : O_2 = 4 : 1$ ) at atmospheric pressure and  $T = 300$  K. Besides its simplicity, the coaxial configuration offers two advantages for the study of streamer dynamics. First, the streamers formed in the coaxial geometry, as shown by the experiments, are predominately 2D, which is much more amicable to this 2D simulation than the typical 3D streamers formed in a pin-type corona discharge. Second, also demonstrated in the experiments [47], the center electrode produces a number of simultaneous, outgoing streamers within one discharge pulse. This behavior is primarily due to a linear ionization instability which drives the initially circular ionization front to become unstable and then break into a number of the disconnected streamers, as illustrated in figure 2(b).

The origin of the linear ionization instability is similar to the fingering phenomena studied in the context of a planar ionization front [34]. As an ionization front propagates under the influence of a constant applied voltage, the gas behind the ionization front becomes highly conductive compared to the non-ionized gas ahead of the ionization front. By voltage division, a larger fraction of the applied voltage is dropped across the non-ionized region as the conductive plasma extends. Therefore, the electric field ahead of the ionization front increases as the ionization front propagates due to this disproportionate distribution of voltage. When a small perturbation causes the ionization front to locally curve slightly outward (locally having a smaller radius of curvature than the rest of the front), this portion of the ionization front will experience an increased electric field in front of it because of the shorter distance between the conductive plasma to the ground electrode. This larger electric field increases the rate of ionization, which accelerates that portion of the ionization front even faster. This instability also applies to the coaxial geometry. Consequently during its radial propagation in the coaxial geometry, the initial circular ionization front will, under slight perturbations, deform and break into a number of streamers, each with a characteristic arrowhead shape (stage 1 to 3 in figure 2(b)).

The initial exponential growth of an infinitesimal perturbation to the ionization front can be characterized by a linear stability analysis. For example, for a *planar* and *negative* ionization front, Arrayas *et al* [34] performed such an analysis to predict ionization instabilities leading to branching. We are not aware of a similar analysis for positive ionization fronts. However, given that the positive ionization front is more nonlinear and depends more critically on non-local phenomena (such as photoionization), it is expected that planar positive ionization fronts would also be intrinsically unstable.

After breaking away from the deformed ionization front, these arrowhead shaped streamers are typically linearly

stable. So the present study will focus on the dynamics of these individual streamers and their nonlinear instabilities under the perturbations of finite amplitudes produced by photon transport. While all the streamers propagate toward the grounded electrode, each can have different strength, speed and life time, thus displaying a variety of different characteristics depending upon the instantaneous and local condition they encounters during propagation. Therefore a single simulation offers opportunity to sample many path-deviation and branching events, just as one observed in the experiments.

The plasma species included in model are the ground states of  $N_2$  and  $O_2$ , the  $N_2$  vibrational states ( $v = 1-8$ ), 3 ground state radicals ( $N$ ,  $O$ ,  $O_3$ ), 5 excited states ( $N_2^*$ ,  $O_2^*$ ,  $N_2^{**}$ ,  $N^*$ ,  $O^*$ ), and 9 charged species ( $e$ ,  $N_2^+$ ,  $O_2^+$ ,  $N^+$ ,  $O^+$ ,  $N_4^+$ ,  $O_4^+$ ,  $O_2^-$ ,  $O^-$ ).  $N_2^*$  is a lumped is populated by electron impact excitation into states lower than  $N_2(b^1\Pi_u)$ .  $N_2^{**}$  is a lumped state populated by electron impact excitation into  $N_2(b^1\Pi_u)$  and higher. The total number of electro-chemical reactions is about 180. To facilitate the propagation of the positive streamers, the photoionization of  $O_2$  by the VUV flux from the radiating  $N_2^{**}$  (the Birge-Hopfield band,  $b^1\Pi_u$ ,  $b^1\Sigma_u^+ \rightarrow X^1\Sigma_g$ ) was included as described below.  $N_2^{**}$  undergoes electron collision quenching (superelastic and ionization collisions) and radiates with an effective lifetime of 5 ns with quenching to lower states also having an effective lifetime of 5 ns.

Secondary electron emission from plasma bounding surfaces due to ion bombardment was included with a secondary emission coefficient  $\gamma = 0.1$ . Secondary electron emission by photon bombardment from the bounding surfaces was neglected for simplicity. The initial electron density in the computational domain is zero except for a small electrically neutral symmetric plasma cloud surrounding the central powered electrode. The electron cloud has a radius of 1.5 mm and peak value of  $[e] \approx 10^{10} \text{ cm}^{-3}$ . This is a thickness of 500  $\mu\text{m}$ . A positive, dc voltage pulse of 50 kV, with 1 ns rise and fall time, was applied to the center electrode to initiate and sustain the streamer discharges. The total number of grid points is about 50 000, of which 44 000 are distributed in the plasma zone with the mesh size varying between 20 and 60  $\mu\text{m}$ . For comparison, identical discharge conditions were used for the simulations with either the existing deterministic or the new statistical photon transport models.

### 3. Dynamics of positive streamers in coaxial configuration

In this section, we discuss results from the model produced by employing the deterministic and statistical photon-transport and ionization algorithms. The causes of path-deviation and branching are discussed from the perspective of disruption of the SCL in the head of the streamer.

Photoionization in the context of positive streamers in air is a complex process that ultimately depends on the details of the transport of resonance radiation emitted by excited states of molecules [22, 48]. Similar to transport of atomic line radiation, photons that are emitted near line center of a vibronic transition terminating on a populated

vibrational state of the ground electronic state are reabsorbed by the ground state leading to radiation trapping. It is the radiation emitted in the wings of the transition or radiation terminating on weakly populated vibrational states that have sufficiently long mean-free-paths to propagate ahead of the streamer to produce ionization. Kulikovskiy estimated that the absorption length of ionization radiation in 1 atm of air is 83  $\mu\text{m}$  [48]. The distributed photon transport model of Zheleznyak *et al* [22] uses a minimum photoionization distance of 33  $\mu\text{m}$  [ $\lambda = 1/(\chi_{\text{max}} p_{O_2})$ ,  $\chi_{\text{max}} = 2 \text{ cm}^{-1} \text{ Torr}^{-1}$ ,  $p_{O_2}$  = partial pressure of  $O_2$ ] and a maximum distance of 1900  $\mu\text{m}$  ( $\chi_{\text{min}} = 0.035 \text{ cm}^{-1} \text{ Torr}^{-1}$ ) for radiation emitted between 980–1025 Å. The absorption length for photoionization has been related to the likelihood for streamer branching. Liu and Pasko [43] found that positive streamers exhibit branching when their radius exceeds the absorption length. They determined that branching will occur when the radius exceeds  $3.5/(\chi_{\text{min}} p_{O_2})$ . This branching occurs due enforcing a Laplacian instability similar to viscous fingering [49]. This mechanism is dominantly a local mechanism. Our interest here is with non-local phenomena. For purposes of demonstration, we have first used a single spectral group for photoionization of  $O_2$  having  $\chi_{O_2} = 0.032 \text{ cm}^{-1} \text{ Torr}^{-1}$  with additional non-ionizing absorption by  $N_2$  having  $\chi_{N_2} = 0.025 \text{ cm}^{-1} \text{ Torr}^{-1}$ . These parameters will admittedly over-emphasize long-mean-free path ionization, however we gain additional insights to the role of the disruption of the space-charge-layer in path deviation and branching. Following this initial discussion, we examine cases having shorter absorption lengths.

#### 3.1. Formation of individual streamers by ionization destabilization

The emergence of individual streamers in the coaxial geometry results from the linear destabilization of the circular ionization front. This destabilization typically undergoes three stages: (1) initially stable circular ionization front, (2) destabilization and distortion of the ionization front and (3) breakaway of individual streamers. Corresponding to the schematics in figure 2(b), the computational results of the initial streamer development are shown in figure 3 using the statistical photon transport model and, for comparison, the deterministic, propagator model. With the statistical model, the initial ionization front, shown by the electron impact ionization rate  $S_e$ , has a circular shape and the circumferential distribution of  $S_e$  is largely uniform with a peak value of  $1 \times 10^{24} \text{ cm}^{-3} \text{ s}^{-1}$ . This circular pattern of the ionization front results from the circular distribution of the initial electron cloud centered at the powered electrode. The ionization front maintains a stable annular shape for about 2 ns with a radial propagation distance of about 1 mm. At  $t = 5$  ns, the linear ionization instability has developed along the ionization front with several ripples appearing along the circumference of the ionization front. The peak value of the  $S_e$  has decreased to about  $8 \times 10^{22} \text{ cm}^{-3} \text{ s}^{-1}$  due to the increasing distance from the center electrode and the resulting decrease in electric field. The circumferential distribution of  $S_e$  has become non-uniform, with peaks located

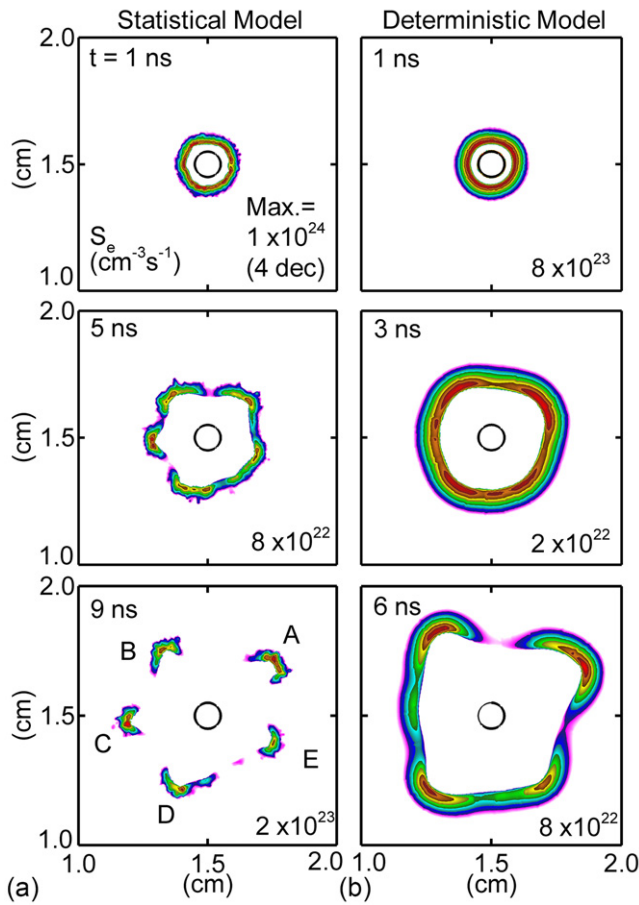


**Figure 3.** The electron impact ionization rate  $S_e$  computed with (a) the statistical photon transport model at  $t = 1, 5$  and  $9$  ns and (b) the deterministic model at  $t = 1, 3$  and  $6$  ns. The dynamics of the streamer emergence are similar for both models up to this point, though those computed by the deterministic model appear to be somewhat smoother. Contours for  $S_e$  are on a log scale over 4 decades.

in the ripple section having a smaller radius of curvature. In contrast, the  $S_e$  in the less curved regions is much reduced as the ionization fronts at these locations dissipate. This dissipation is exacerbated by a shorting out of the local electric field by the more conductive plasma in the more rapidly advancing ionization fronts. At  $t = 9$  ns, the instability has developed further and the ionization front is separated into a number of individual streamers (A–E). Spatially separate, the individual streamers propagate radially outward but with different shapes, although a general arrowhead shape can be identified. At this point, the streamers have traveled about 3–4 mm, about half the distance between the electrodes. Due to the shorter distance to the ground electrode and compression of voltage from the conductive regions into the non-ionized regions ahead of the streamer, the peak values of the  $S_e$  in the individual streamers increased to  $2 \times 10^{23} \text{ cm}^{-3} \text{ s}^{-1}$ .

Note that the process by which individual streamers emerge out of the initial circular ionization front is due to the intrinsic linear instability, and not the statistical nature of the photon transport. It takes some propagation distance for the instability to occur. As the ionization front propagates to a larger radius, the front appear more planar and so

becomes more sensitive to the instability. To compare,  $S_e$  from an otherwise identical simulation using the deterministic propagator photon transport are shown in figure 3(b). The three stages of formation of individual streamers can still be identified at  $t = 1, 3$  and  $6$  ns, similar to those for the statistical photon transport. The shapes of the ionization fronts, and order of the magnitude of the peak values of the  $S_e$  are quite similar to the statistical model. The ionization rates are  $8 \times 10^{23} \text{ cm}^{-3} \text{ s}^{-1}$  in the stable regime,  $2 \times 10^{22} \text{ cm}^{-3} \text{ s}^{-1}$  in the destabilization regime and  $8 \times 10^{22} \text{ cm}^{-3} \text{ s}^{-1}$  in the individual streamer regime. The timings between the statistical and deterministic models are different, with the statistical model lagging behind the deterministic model by a few ns. This is due to a longer induction time required to launch the ionization wave when using the statistical model.

The individual streamers formed at  $t = 6$  ns with the deterministic model are smoother and more elongated in the circumferential direction, reflecting the characteristics of the propagator photon transport model with instantaneously isotropic photon fluxes. These results show that the mode of photon transport, statistical or deterministic, has only a minor effect on the large scale formation of the individual streamers which primarily result from linear destabilization of the ionization front. The triggering of the linear destabilization in the experiments could come from deviations from the exact shape and surface property of the electrodes, small fluctuations in gas density or composition due to flow or dust, or small variations in the initial electron density resulting from the previous pulse. In the simulations, the destabilization is likely due to the discrete nature of the mesh, finite convergence criteria in the linear algebra routines or numerical round off errors. However, as will be shown below, after the individual streamers form, photon transport has a major effect on their propagation dynamics. Note there is one significant difference between the statistical and deterministic models—the individual streamer C produced in the deterministic treatment is much weaker than in the statistical model.

To further compare the statistical and deterministic photon transport models, the photon-ionization rates  $S_p$  at the same times as for  $S_e$  are shown in figure 4. During the 3 stages of the linear destabilization, the overall shapes and magnitudes of  $S_p$  from the two models are quite similar. The results of  $S_p$  from the deterministic model can be considered as an averaged or smoothed version of the photoionization rates from the statistical model. The  $S_p$  from the statistical model initially shows fine grain structure but no preferred direction, reflecting the stability of the statistical sampling in the implementation of the model. For both the statistical and deterministic models, the maxima of  $S_p$  in the first two stages of destabilization are close to the center electrode, due to the exponential photon absorption rate along the radial direction *before* the individual streamers form. However, once the streamers break away in stage 3, the peaks of  $S_p$  shift to the streamer heads. At this point, the peak magnitude of  $S_p$  for the deterministic model,  $5 \times 10^{21} \text{ cm}^{-3} \text{ s}^{-1}$ , is about a quarter that for the statistical model,  $2 \times 10^{22} \text{ cm}^{-3} \text{ s}^{-1}$ . This difference reflects the difference between the spatially averaged value of  $S_p$  in the deterministic model and the local instantaneous value of  $S_p$

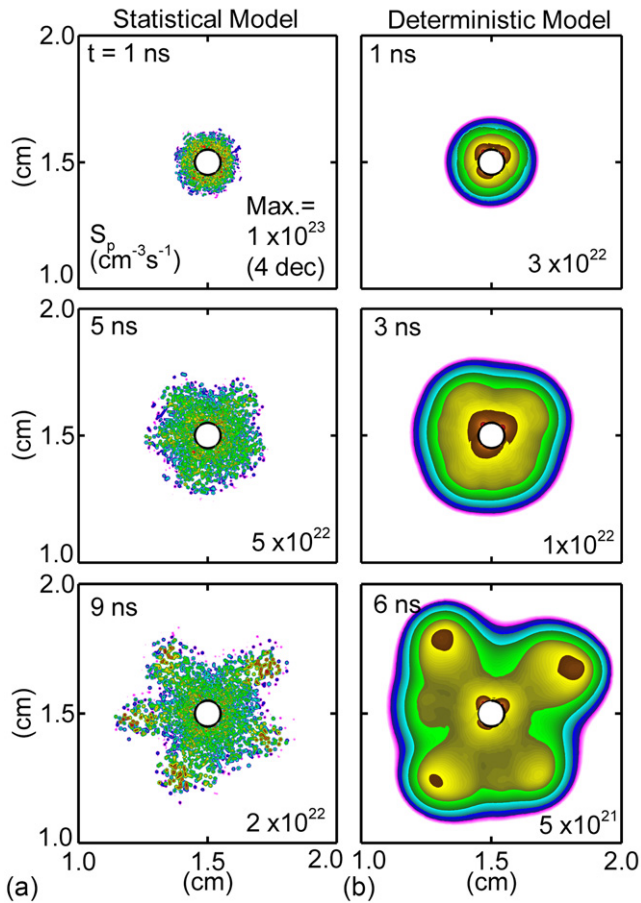


**Figure 4.** The photoionization rates  $S_p$  computed with (a) the statistical photon transport model at  $t = 1, 5$  and  $9$  ns and (b) the deterministic model at  $t = 1, 3$  and  $6$  ns. The overall characteristics of  $S_p$  are similar for both models. The deterministically produced  $S_p$  may be regarded as a spatially averaged version of the statistically produced  $S_p$ . Contours are on a log scale over 4 decades.

in the statistical model. The close resemblance of distribution and magnitudes of  $S_p$  between the two models suggests that the statistical photon transport model is a reasonable discretized version of the deterministic propagator model. Note, however, that 5 streamers form when using the statistical model but only 4 streamers form when using the deterministic model, to be discussed below.

Once the individual streamers form, they tend to be linearly stable, and can maintain their typical arrowhead shape, even in the presence of small perturbations, all the way to the ground electrode. This stable mode of propagation has been shown in many previous simulations of the individual streamers and is confirmed in the present simulations with the deterministic photon model. For example, the electron density  $n_e$ , net space charge density  $\rho$  and the instantaneous photoionization rate  $S_p$  of the streamers as produced by the deterministic photon transport model at  $t = 8.5$  ns are shown in figure 5. The four individual streamers produced by the destabilization of the ionization front each propagate toward the ground electrode in essentially a radially outward directly. Each streamer maintains a smoothly curved ionization front. The streamers are, however, perturbed by their neighboring streamers and travel at different speeds due to a shorting

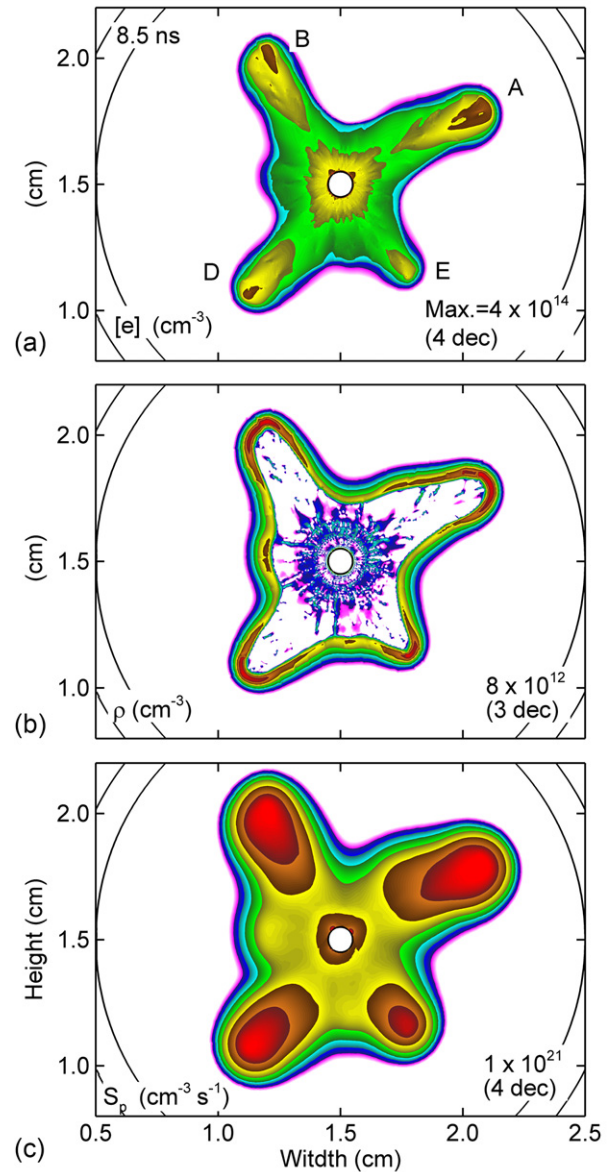


**Figure 5.** Streamer properties obtained with the deterministic photoionization model at  $8.5$  ns. (a) electron density  $n_e$ , (b) space charge density  $\rho$  and (c) photoionization rate  $S_p$ . Four streamers (A, B, D and E—see figure 1) are produced which propagate in a stable fashion with arrowhead shaped SCLs. Contours are on a log scale with the number of decades shown in each frame.

of the electric potential by the conductive channel produced by a neighbor. For example, streamer D was initially produced somewhat ahead of streamer E. The conductive channel produced by streamer D reduced the electric field in the vicinity of streamer E, thereby slowing streamer E. In the absence of significant perturbations, as might occur by statistical photoionization, the individual streamers produced by the linear destabilization of the ionization front do not branch.

The electron density  $n_e$ , net charge density  $\rho$  and the instantaneous photoionization rate  $S_p$  of the streamers at  $t = 12.8$  ns are shown in figure 6 for the statistical model. In this particular case, there are 5 primary streamers, labeled from A to E in figure 5(a) and which correspond to the

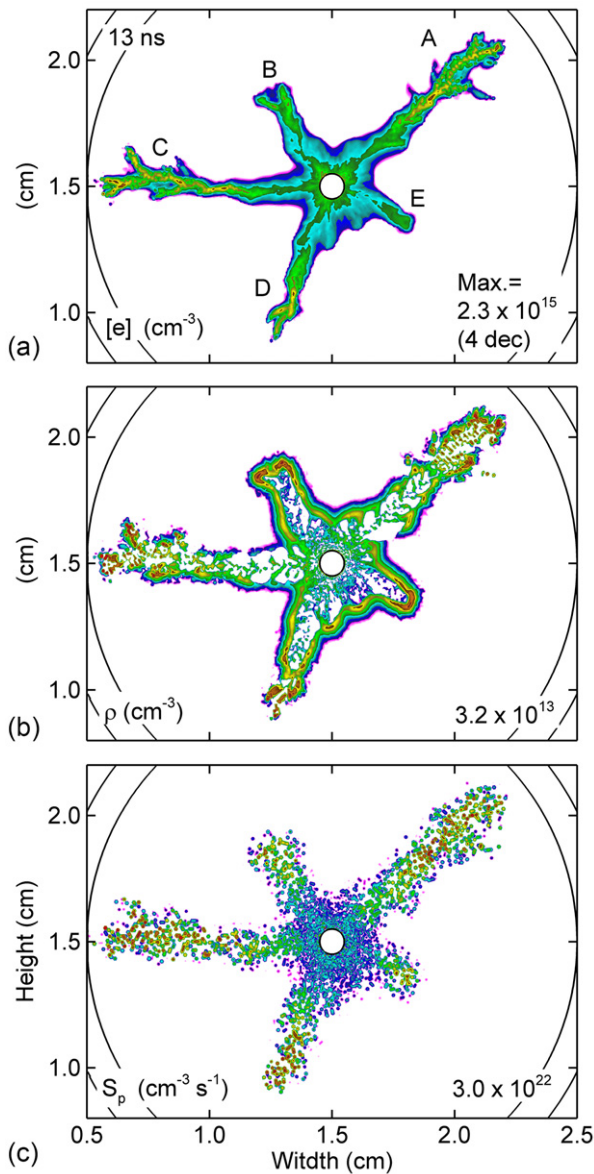


**Figure 6.** The propagation, path-deviation and branching of individual streamers from the statistical photon transport model shown by (a) electron density  $n_e$ , (b) space charge density  $\rho$  and (c) photoionization rate  $S_p$  at  $t = 12.8$  ns. Of the five individual streamers, four (A–D) show path-deviation and branching, while streamer E propagates as a single structure. The branching is associated with the breaking of the space charge layer (SCL). Contours are on a log scale over 4 decades.

destabilized streamers in figure 3(a). All streamers propagate approximately in the radial direction. However, they have significantly different propagation speeds and shapes that differ from the deterministic model. The streamers display: regular propagation, path-deviation and branching. The slowest streamer, E, is basically following a radial trajectory without significant change with a decreased speed caused by a shorting of the electric field by the presence of the adjacent faster streamers that have trailing conductive columns. This slowing was also seen in the deterministic model. The streamers A–D all display multiple branchings and path-deviations during their propagation. These different behaviors result from the

specific ways that the SCL at the streamer head interacts with the local gas and plasma region in front of it due to the statistical nature of electrons seeded by transport of ionizing radiation from the plasma trailing behind.

The SCLs of these streamers are shown in figure 6(b). The SCLs tend to mark the boundary between the plasma and the neutral gas. In this case, the SCLs border the conductive channels trailing the streamer heads that are filled by the quasi-neutral plasma. Streamer E has a regular and continuous semi-circular SCL at the streamer head with a high  $\rho$  on the order of the  $10^{13} \text{ cm}^{-3}$ . It is this charge density that produces the electric field that continues to avalanche the streamer head. The SCL at the streamer head extends into SCLs bordering the conductive channel in which  $\rho$  is about one order of magnitude smaller than in the head. This lower SCL produces the confining ambipolar field in the transverse direction to propagation.

Branching takes place in streamers A to D, each having morphed from a primary, stem-like streamer into a tree-like structure with two or more branches at different locations. For example, at the head of the streamers B and D, the SCLs have broken into two or more pieces due to large disturbances produced by the statistical photoionization. The broken SCLs at the streamer heads strongly contrast with the continuous SCLs trailing behind the heads, which mark the boundaries of the plasma channels formed up to this point. For streamers A and C, the breaking of the SCLs has taken place several times. Each newly broken piece of the SCL is associated with some of the highest values of  $\rho$  at this moment, and thus could develop into a new local streamer. Broken SCLs constitute a primary source of streamer branching.

The five branches of the instantaneous photoionization rate  $S_p$  are shown in figure 6(c). The  $S_p$  in the center circular region is reminiscent of the initial circular isotropic phase of propagation before destabilization and before the individual streamers emerge. Here we note two important characteristics of the  $S_p$ . First, the peaks of  $S_p$ , around  $3 \times 10^{22} \text{ cm}^{-3} \text{ s}^{-1}$ , are located near the tips of the spokes, not in the hub region at small radius. This is primarily due to the finite life time of the excited species, which is in present case about 5 ns. So the excited states in the hub region at this point (about  $t = 13$  ns) have been mostly relaxed through photon emission or collisional quenching. Second, although the five primary streamers A to E can be identified with the five spoke-like regions in  $S_p$ , the instantaneous  $S_p$  in these regions is rather statistically smooth. From the spatial distribution of  $S_p$  alone, it is not clear whether a particular streamer has branched or not. For example, the  $S_p$  at the tip of regular, non-branching streamer E is not so different from those at the clearly branched streamer B. This suggests that the branching is not merely due to the randomness of the photo-electron seeding alone, rather it results from an active interaction between the SCLs at the streamer heads and the random photon-electron seeding in front of them.

After the destabilization phase of streamer propagation, the deterministic model produces four streamers (figure 5(a)) whereas the statistical model launches 5 streamers (figure 6(a)). The deterministic case is missing streamer C. The cause for this disparity is the ability of the statistical model to

produce seed photoionization beyond the horizon of photoionization produced by the deterministic model. In this particular case, the adjacent streamers B and D reduce the magnitude of the electric field in the location of streamer C by producing adjacent electrically conductive regions. With the deterministic model, the magnitude of photoionization provided in this low electric field region was too small to sustain the proto-streamer generated by the destabilization. The end result is that the proto-streamer dies out. The statistical photoionization model randomly produced a seed of electron density at a larger radius where the electric field is larger, which could then initiate avalanche. The end result is that the proto-streamer was able to propagate into a full streamer.

### 3.2. Path-deviation of streamer propagation

Abrupt changes in the direction of propagation of the streamer, or path-deviation, are shown in figure 6(a) by the zig-zag shape of the primary plasma channels. These path-deviations are associated with deformation of the SCL from a *symmetric* arrowhead shape to an *asymmetric* shape. This process is demonstrated by the electron density  $n_e$  and space charge density  $\rho$  in figure 7 for the statistical model streamer D at  $t = 9.0$  and  $11.4$  ns. These times are before and after the streamer undergoes a path-deviation event. At  $t = 9.0$  ns, with a maximum value of  $n_e \approx 1 \times 10^{14} \text{ cm}^{-3}$ , the streamer propagates from the right to the left, nearly horizontally but slightly downward, as indicated by the arrow. The lines of equipotential in front of the streamer head are bent around the highly conductive channel produced by the streamer and bent around the SCL in the head of the streamer. The curvature of the bending is determined by the radius of the streamer head in the transverse direction. The corresponding SCL in figure 7(b) has an arrowhead shape pointing to the left with peak value of  $\rho \approx 2 \times 10^{13} \text{ cm}^{-3}$ , located at the vertex of the SCL. The two trailing edges of the SCL are approximately symmetric about the direction of propagation direction and share the peak  $\rho$  at the vertex. This configuration of the SCL helps maintain the direction of the streamer propagation and produces, up to this time, a stable and relatively straight plasma channel behind the streamer head. Note that there is some statistical noise in the values of both  $n_e$  and  $\rho$ , a consequence of the statistical production of photoionization that seeds the propagation.

By  $t = 11.4$  ns, the streamer head has moved further to the left and has made an abrupt change in its direction of propagation. The streamer formally was moving to the lower-left and is now moving to the upper-left, as shown by the arrows. The configuration of the SCL is the cause of the path-deviation. In contrast with the shape of the SCL at  $t = 9$  ns, the two trailing legs of the SCL from the vertex have at this point become asymmetric with respect to the *original* direction of propagation and they no longer share a common peak of  $\rho$  at the vertex. The upper leg of the SCL, with a peak  $\rho \approx 2 \times 10^{13} \text{ cm}^{-3}$ , has become stronger than the lower leg whose peak values is now  $\rho \approx 9 \times 10^{12} \text{ cm}^{-3}$ . This broken symmetry in the SCL causes the streamer to change its direction of propagation. The symmetry is broken by a statistically larger source of ionization ahead and above the

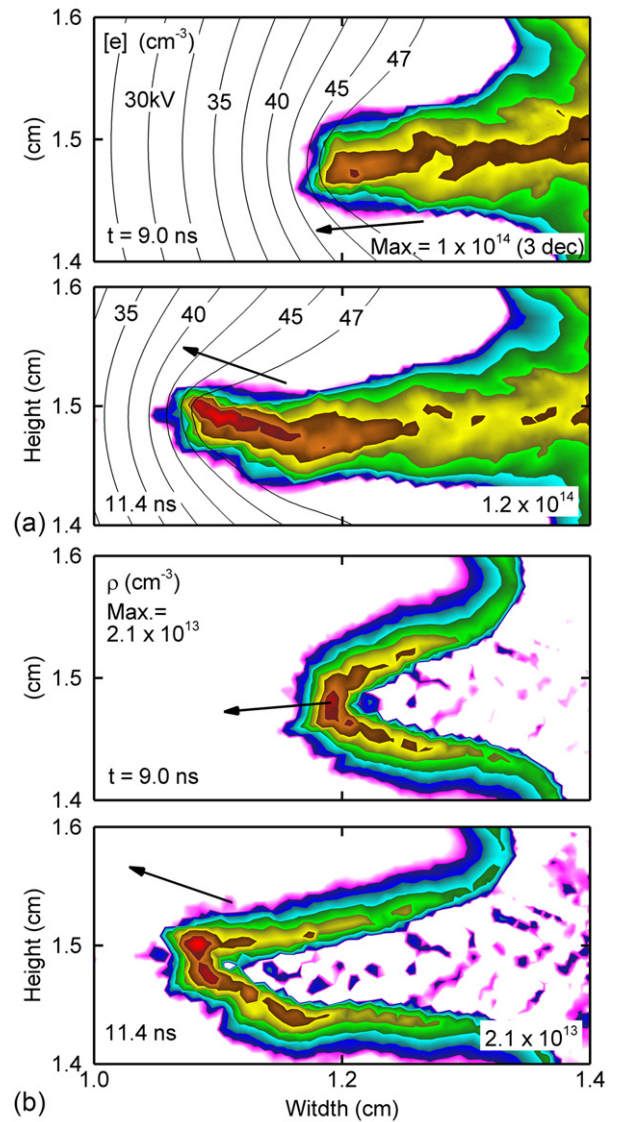


**Figure 7.** The path-deviation during streamer propagation shown by (a) electron density  $n_e$  with electric potential contours, and (b) space charge density  $\rho$  for streamer C at  $t = 9.0$  and  $11.4$  ns. The abrupt change of the direction of propagation, shown by the arrows, is associated with the transition of the SCL from a symmetric shape to an asymmetric shape. Contours are on a log scale over 3 decades.

streamer, which avalanches to produce a larger  $\rho$ . Repetitive occurrences of symmetry-breaking of the SCL by this random seeding of electrons by photoionization can produce a zig-zag shape of the plasma channels, as shown in figure 6(a).

### 3.3. Streamer branching

Although during the path-deviation, the symmetry of the SCL is broken, its topology generally remains the same. That is, the SCL may be perturbed but it remains continuous. If, on the other hand, the topology of the SCL changes, that is the SCL is broken into two or more disconnected pieces, then streamer branching may take place. The details of the breaking process of the SCL for streamer B are shown in figure 8 by the electron density  $n_e$  and space charge density  $\rho$  at times of  $t = 11$ ,  $12$ , and  $13$  ns. At  $t = 11$  ns, the primary

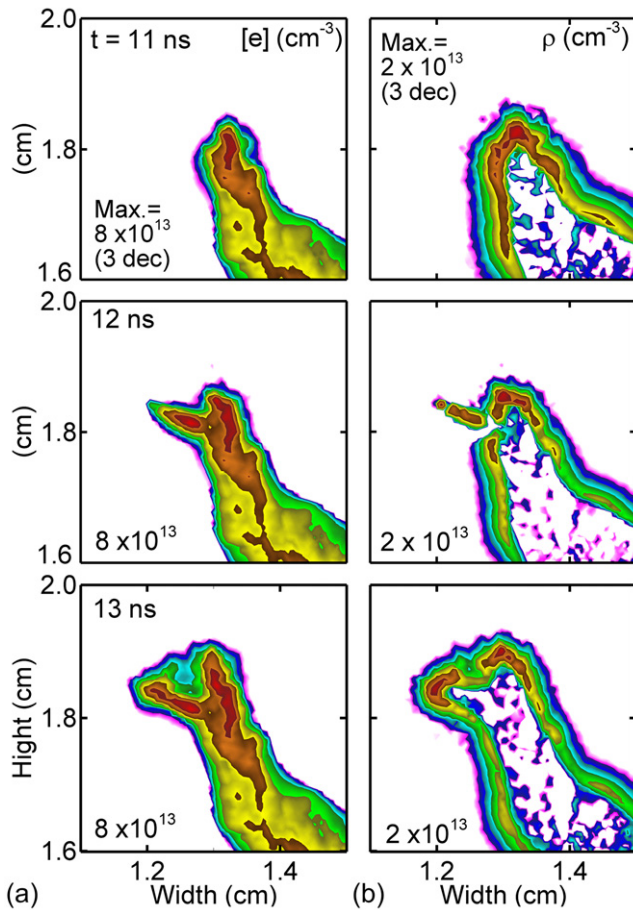


**Figure 8.** The streamer branching process shown by (a) electron density  $n_e$  and (b) space charge density  $\rho$  for streamer B at  $t = 11$ , 12 and 13 ns. The branching of a primary streamer is through the breaking of its SCL by the collision with a secondary streamer. The secondary streamer is initiated remotely by stochastic photoionization but avalanches toward the primary streamer, see  $n_e$  and  $\rho$  at  $t = 12$  and 13 ns. Contours are on a log scale over 3 decades.

streamer is propagating upward and is not branched, although it has experienced some path-deviation. The SCL, shown by  $\rho$ , is arrowhead shaped and is contiguous. At  $t = 12$  ns, a separate secondary streamer head has developed ahead and to the left of the primary streamer and connects with the primary streamer from the upper-left. The SCL has an isolated island corresponding to the secondary streamer and is not contiguous. At  $t = 13$  ns, two separate streamer branches have formed and propagate in different directions. The initially nearly straight plasma channel produced by the head of the primary streamer up to  $t = 11$  ns has now morphed into a two-prong Y-shaped plasma channel. During this process, the peak electron density,  $n_e \approx 8 \times 10^{13} \text{ cm}^{-3}$ , does not significantly change. However, as indicated by the locations of the local maxima in  $n_e$ , the new secondary branch does not grow from the primary streamer itself. Rather the secondary branch originates outside the primary streamer and then propagates toward it. This new branch was initiated by a photoionization event that statistically occurred far enough ahead and to the left of the streamer in a sufficiently large electric field that an avalanche could be sustained.

The relationship between the streamer branching and the change of the topology of the SCL is shown in figure 8(b). Up to  $t = 11$  ns, the SCL maintains a connected, contiguous arrowhead shape with a slight asymmetry about its direction of propagation caused by a recent path deviation. By  $t = 12$  ns, the secondary streamer has emerged from the upper left due to production of seed electrons by photoionization and propagates toward the primary streamer. The secondary streamer produces a strong perturbation to the primary streamer when the SCL of the secondary streamer intercepts the SCL of the primary streamer. This perturbation breaks the SCL of the primary streamer into two pieces. Here, the secondary streamer is anode-directed where the primary streamer head serves as the virtual anode. The emergence of the positive SCL in the secondary streamer results from the rapid acceleration and thus depletion, of the avalanched electrons in the secondary streamer toward the head of the primary streamer. The breaking of the primary SCL upon collision with the backward secondary streamer results from the injection of these electrons from the secondary streamer into the positive SCL of the primary streamer. There is simply neutralization of the positive space charge due to the injection of the electrons but there is also additional electron–ion recombination. In this particular configuration, the SCL of the secondary streamer merges with the lower fragment of primary SCL, while the upper fragment remains largely unaffected. By  $t = 13$  ns, two individual streamers have emerged from the collision, each with an arrowhead shaped SCL. The two branched streamers propagate in different directions due in part to the mutual repulsion of their respective positive SCL. At this point, the streamer branching has been completed. The primary streamer continues upward whereas the secondary streamer moves to the left. Throughout the branching process, the magnitude of the space charge density within the SCLs remains largely the same,  $\rho \approx 2 \times 10^{13} \text{ cm}^{-3}$ . So the branching is not so much due to a sudden change in the magnitude of the SCL. Rather, the branching is due to the change of the topology of the SCL, from contiguous to non-contiguous, or broken.

To summarize, a feature of this streamer branching mechanism is that the new streamer is first initiated outside the primary streamer, after which the secondary streamer avalanches toward and finally collides with the primary streamer. The emergence of the secondary streamer outside the primary streamer results from a combination of the electron seeding by non-local photoionization and a high enough electric field produced by the SCL of the primary streamer at the seeding location at this particular moment.

The backward propagating secondary streamer which originates from the random seeding of the photo-electrons, and their interaction of the secondary streamer with the primary streamer cause disruptions to the SCL of the primary streamer. Depending on the intensity of the disruption, such interactions can result in either an abrupt path-deviation when the symmetry of SCL is altered but the SCL remains contiguous, or a branching event when the topology of the SCL is changed by breaking into two or more pieces. These processes can occur repeatedly in time and space during the propagation of a streamer, thus producing multi-level branching or more than

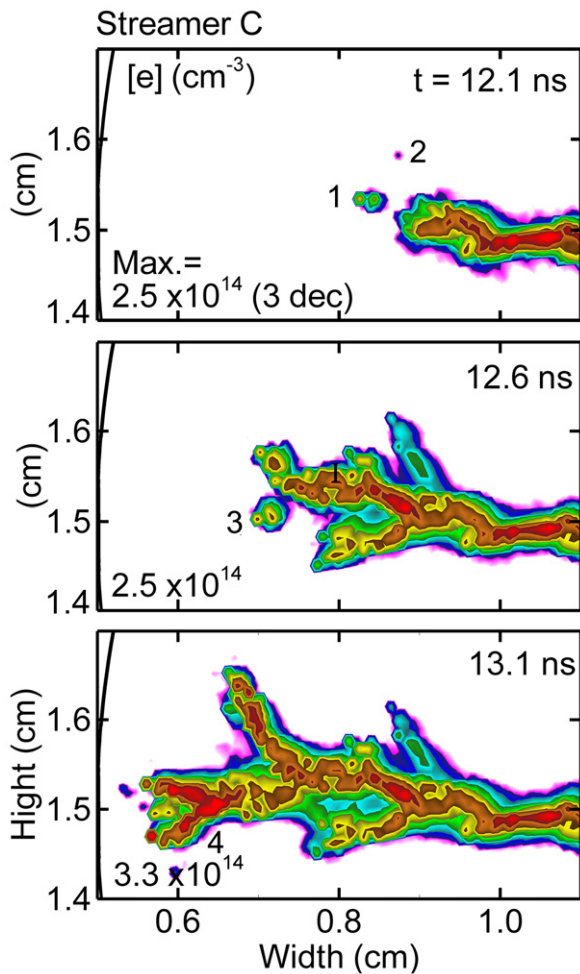


**Figure 9.** Consecutive streamer branching to form a multi-level tree-like structure, shown by the electron density at  $t = 12.1$ ,  $12.6$  and  $13.1$  ns for streamer C. Contours are on a log scale over 3 decades. The numbers within the figure refer to locations highlighted in the text.

two branches in one event [50]. This compound branching process is demonstrated by the electron density for streamer C at  $t = 12.1$ ,  $12.6$  and  $13.1$  ns in figure 9, and for streamer D at  $t = 12.6$ ,  $12.9$  and  $13.1$  ns in figure 10. Streamer C undergoes a sequence of branching producing 2 streamers with each event. Streamer D experiences a single event that produces 3 branches. We emphasize that although complex, tree-like streamer structures can result from the compound process, the unit cell of such tree-like structure, path-deviation and branching, follows essentially the same dynamics discussed above—random seeding of photoelectrons, backward propagating avalanche of a secondary streamer, collision with the primary streamer and disruption of the SCL of the primary streamer.

The left-bound primary streamer in figure 9(a) shows a zig-zag pattern at  $t = 12.1$  ns due to path-deviation but branching has not taken place at this time. However an initial small electron cloud appears ahead of the primary streamer head (at location 1) due to a photoionization event. In other words, this small cloud of plasma results from a discrete photoionization event which happened to be in the region having a large enough electric field to support further

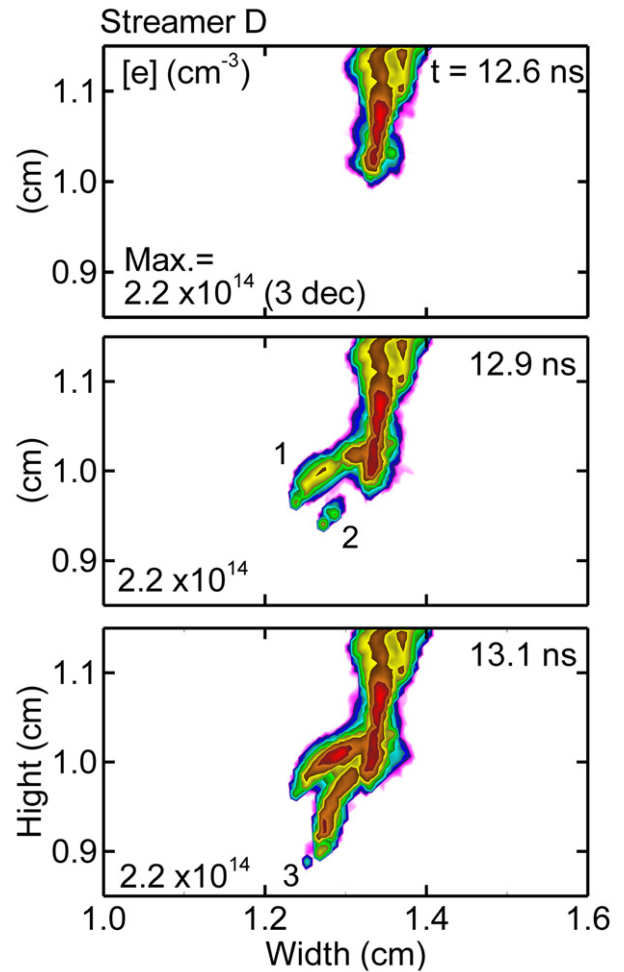


**Figure 10.** Consecutive streamer branching to form a three-pronged structure, shown for streamer D at  $t = 12.6$ ,  $12.9$  and  $13.1$  ns. Contours are on a log scale over 3 decades. The numbers within the figure refer to locations highlighted in the text.

ionization. There are many additional such ionization events that occur in regions that do not support additional avalanche. Those electron seeds dissipate largely by attachment to  $O_2$ . There is one such seed visible in figure 9(a) at location 2 to the upper right of location 1 that nearly dissipates but is able to launch a weak streamer which forms a branch that does not continue. By  $t = 12.6$  ns, the seeding electron cloud has developed into a separate (upper) branch through a backward avalanche and connection with the primary streamer. The same process also occurs for the lower branch (though its seeding electron density is too low to be seen here). As a result, the primary streamer at  $t = 12.6$  ns forks into two branches. At the same time, there are also new seeding electrons appearing below the upper branch (at location 3) which then repeats the same process and develops into a new lower branch at  $t = 13.1$  ns. At this juncture, the tip of this newly developed lower branch experiences further branching, as shown by the rightmost part of the streamer around at location 4 near  $0.6$  cm. This sequential branching process produces a multi-level, tree-like structure of the streamer, which resembles those often observed in natural lightning and lab experiments.

A similar time sequence is shown in figure 10 which produces a three-pronged streamer head for streamer D.

At  $t = 12.6$  ns streamer D is a singular, downward propagating streamer. At  $t = 12.9$  ns, a new branch develops to the left (location 1), forming a two-pronged streamer head. Meanwhile, remote sites are photoionized (location 2), from which a new avalanche starts forming the third prong that joins the already branched streamer head at  $t = 13.1$  ns [50]. A spot of remote ionization at location 3 is the precursor for a small path deviation. Throughout this sequential process, the magnitudes of  $n_e$  and  $\rho$ , both around  $10^{14} \text{ cm}^{-3}$ , change only modestly. During the branching process, the secondary streamers branching from the primary streamer quickly reach nearly the same plasma density and SCL density as the primary streamer. This enables a continuation of the branching process into multi-levels without a premature termination as long as there is sufficient voltage available ahead of the streamer to enable avalanche. Had the new streamers been much weaker compared to their predecessors the branching might terminate.

From a statistical point of view, a larger photoionization source always occurs on average or with a higher probability in the close vicinity of a photon emission point than at distant locations. However, at any given instant, statistically photons can be absorbed at remote locations from the streamer head while leaving closer regions in between without photoionization. Individual avalanches can then originate from these remote sites either due to the local electric field being critically large or due to the approaching high electric field associated with the SCL of the streamer head. There is, then, an optimum distance from the streamer head to produce a secondary streamer that will produce a branching. Once the avalanche starts in the secondary streamer, the ionization wave will tend to propagate toward the primary streamer. The gradient of the electric field is positive toward the primary streamer and the closer to the head of the primary streamer the more pre-ionization the secondary streamer will find. This sequence emphasizes the importance of appropriate locations of the photoionized electron seeding to produce branching. If the seeding photoionization is too far from the primary streamer, an avalanche may not be sustainable because the local electric field may be too low. If the seeding photoionization is too close to the primary streamer, the electric field may be large enough to avalanche, however the distance to the primary streamer may be too small for the avalanche to grow into a separate streamer. So in this case, the new avalanche will simply merge with the primary streamer rather than produce a strong disturbance to the SCL of the primary streamer. These two bounding factors stress the probabilistic nature of streamer path-deviation and branching.

The proposed mechanism for streamer path-deviation and branching discussed above has been further checked by carrying out a number of simulations with varying statistical parameters. These parameters include using finer (doubling the number of mesh points) and coarser meshes, changing the seeds for the random number sequences, changing the number of subdivisions in angle and distance surrounding an emission site and changing the size and location of the initial electron clouds. We conclude from these numerical tests that the process of random, remote photo-electron seeding,

development of a back-running avalanche, collisions between the secondary and primary streamers, and the distortion and topology change to the SCL of the primary streamer represents a statistically robust dynamical mechanism that may explain many aspects of streamer path-deviation and branching.

The propensity for branching and path deviation is a function of the magnitude of the electric field ahead of the streamer. The larger the electric field ahead of the streamer, the higher the likelihood that an electron avalanche will be initiated by a remote photoionization. The electric field ahead of the streamer is determined in part by the conductive plasma column of the streamer which has a small voltage drop and so compresses the applied voltage in the non-ionized region ahead of the streamer. In this regard, individual streamers affect their neighbors through this shorting of the electric potential. For example, the  $E/N$  and electron density are shown in figure 11 for conditions similar to those just described. As the individual streamers propagate from the powered electrode toward the grounded electrode, each produces a conductive channel having low  $E/N$  and a space charge enhanced  $E/N$  at the head of the streamer. Those streamers which are statistically faster than their neighbors reduce the  $E/N$  ahead of the streamer for their neighbors, which slows their propagation. As the faster streamers approach the grounded electrode, the  $E/N$  ahead of the streamer increases, which then promotes a higher rate of branching (see the top-right streamer). Upon reaching the grounded electrode, a negative ionization wave restrike occurs, which follows the circuitous path of the branching.

To investigate the effect of the intensity and the mean-free-path of the photoionization radiation, additional simulations were performed. In the first two cases, the non-ionizing absorption by  $\text{N}_2$  was increased to  $\chi = 0.05 \text{ cm}^{-1} \text{ Torr}^{-1}$  and  $0.1 \text{ cm}^{-1} \text{ Torr}^{-1}$ . This increase in non-ionizing absorption has the effect of reducing both the intensity and the range of the photoionizing radiation. It is difficult to perform side-by-side comparisons of these cases. The branching is dominated by stochastic processes that result in significantly different structures in each case. For example, the orientations and number of streamers in each case differ. Nevertheless, the fundamental mechanisms discussed above concerning the SCL do not change.

Selected branchings are shown in figure 12 for non-ionizing absorption by  $\text{N}_2$  having  $\chi_{\text{N}_2} = 0.025, 0.05$  and  $0.1 \text{ cm}^{-1} \text{ Torr}^{-1}$ . The streamers have been rotated from their original orientations to enable comparison. With an increase in  $\chi_{\text{N}_2}$  there is less total photoionization due to the increase in the non-ionizing absorption. As a result, the overall streamer structure propagates slower. With  $\chi_{\text{N}_2} = 0.025 \text{ cm}^{-1} \text{ Torr}^{-1}$ , the fastest streamer branch reaches the outer grounded electrode in 13.2 ns. With  $\chi_{\text{N}_2} = 0.1 \text{ cm}^{-1} \text{ Torr}^{-1}$ , the grounded electrode is reached in 17.8 ns. As the magnitude and range of the photoionization decreases ( $\chi_{\text{N}_2}$  increases), the branching becomes more filamentary. As the photoionization seeds become more sparse and of lower magnitude, and on a relative basis, more ionization occurs closer to the streamer, the onset of branching becomes more statistical, as there must be a favorable local electric field to initiate the daughter streamer.

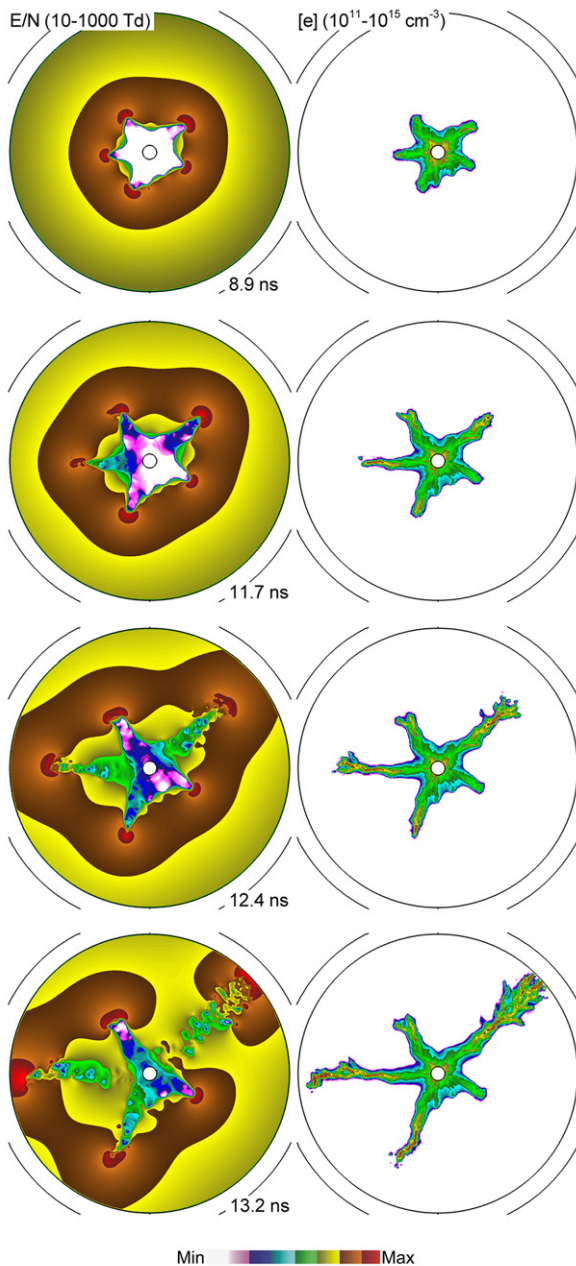


**Figure 11.** Electric field (left) and electron density (right) for increasing times after application of voltage. Propagation of individual streamers at different speeds affects the electric field ahead of neighboring streamers. Fast propagating streamers will slow the propagation of neighboring streamers and reduce their likelihood for branching and path deviation.

Another parametric study was performed in which the non-ionizing absorption was retained at  $\chi_{N_2} = 0.025 \text{ cm}^{-1} \text{ Torr}^{-1}$ . In the first case, the photo-ionizing absorption cross section for  $O_2$  was increased to  $\chi_{O_2} = 0.096 \text{ cm}^{-1} \text{ Torr}^{-1}$ . In the second case, two groups of photons were used. The first group has  $\chi_{O_2} = 0.032 \text{ cm}^{-1} \text{ Torr}^{-1}$  representing radiation in the wings of the line, and which receives 10% of the VUV emission. The second group has  $\chi_{O_2} = 0.32 \text{ cm}^{-1} \text{ Torr}^{-1}$  representing radiation in the center of the line, and which receives 90% of the VUV emission. Quenching of  $N_2^{**}$  by  $O_2$  has rate coefficient

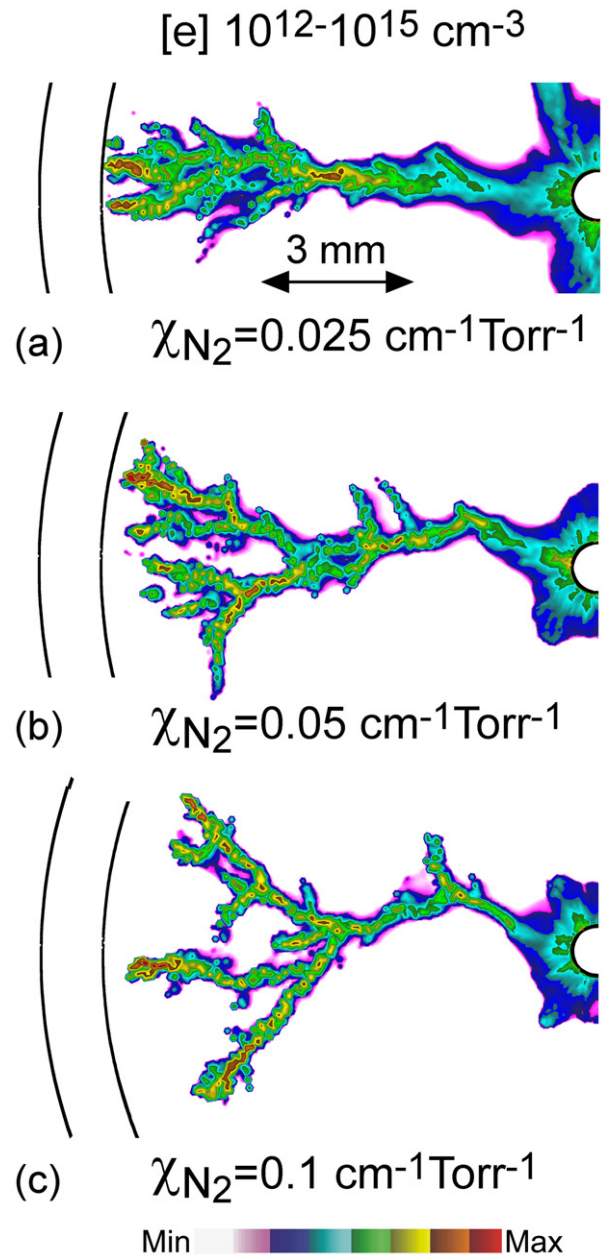


**Figure 12.** Selected streamers (rotated to the same orientation) for non-ionizing absorption by  $N_2$  having absorption coefficient (a) 0.025, (b) 0.05 and (c)  $0.1 \text{ cm}^{-1} \text{ Torr}^{-1}$ . Increasing non-ionizing absorption localizes ionization closer to the streamer and produces more filamentary structures.

$3 \times 10^{-10} \text{ cm}^3 \text{ s}^{-1}$  [51]. For these cases, the plasma was initiated by a single spot of plasma with its center on the surface of the powered electrode, having a density of  $5 \times 10^9 \text{ cm}^{-3}$  and radius of  $75 \mu\text{m}$ . Selected branchings are shown in figure 13, also rotated to enable comparison. The overall structures of the branchings are similar to prior cases. The branching is perhaps more filamentary for the case using 2-photon groups where the majority of the photoionizing absorption occurs with a shorter mean-free-path. A recurring trend is that shortening the mean-free path for photoionization (or localizing the photoionization closer to the streamer) produces a more filamentary structure with fewer branches. However, any

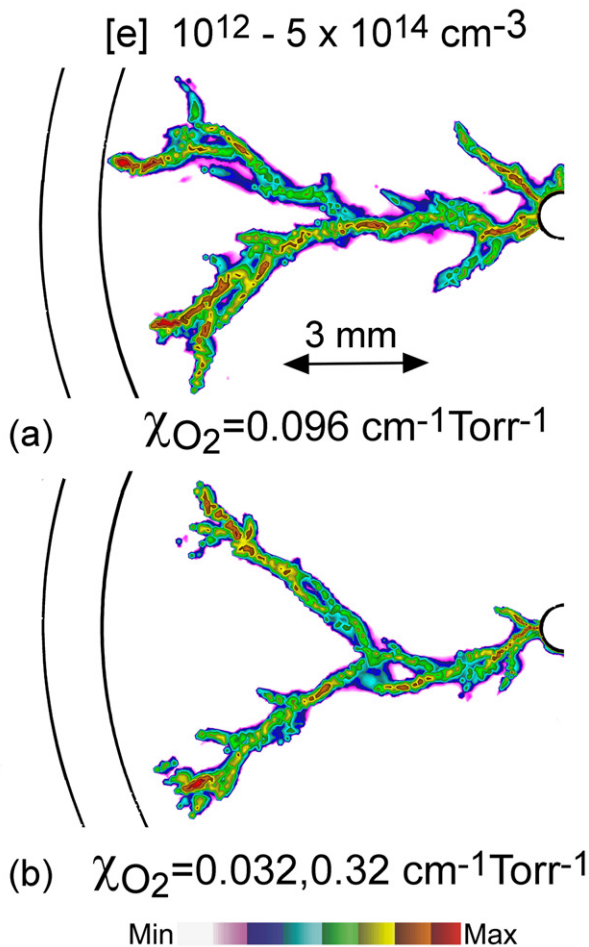


**Figure 13.** Selected streamers (rotated to the same orientation) for different photoionizing absorption by  $\text{O}_2$ . (a) A single photon group having  $\chi_{\text{O}_2} = 0.096 \text{ cm}^{-1} \text{ Torr}^{-1}$ . (b) 2-photon groups having  $\chi_{\text{O}_2} = 0.032 \text{ cm}^{-1} \text{ Torr}^{-1}$  and  $0.32 \text{ cm}^{-1} \text{ Torr}^{-1}$ .

long mean free path photoionization that produces electrons in a random or stochastic manner remotely from the head of the streamer will produce some form of path deviation or branching if, the local electric field is sufficiently intense.

#### 4. Concluding remarks

The branching and path-deviation of positive streamers in molecular gases such as air likely require a statistical process which destabilizes the space charge layer (SCL) of the streamer head from a generally symmetric, contiguous configuration to an asymmetric, broken configuration. In this paper, mechanisms for path-deviation and branching of atmospheric pressure positive streamer discharges in air were discussed based on results from a numerical investigation from the viewpoint of statistical photon transport and photoionization. A statistical photon transport model was developed to account for the particle nature of ionizing photon transport at the head of streamers. This statistic model for photoionization was embedded into a continuum and otherwise deterministic model for plasma hydrodynamics. The large scale behavior of the streamer (scale lengths large compared to the radius of the streamer head) produced by the statistical model approximates

that produced by an otherwise identical plasma model using a deterministic photon transport model. However, on the scale length of the streamer head, there are significant differences between the models.

It was found that the dynamics of the streamer propagation, path-deviation and branching are largely controlled by the thin SCL at the head of the streamer. During the propagation of a primary streamer, secondary streamers initiated ahead the primary streamer by statistical photoionization can initiate a new electron avalanche that propagates backward toward the primary streamer head. Upon collision of the locally anode directed secondary streamer with the primary streamer, the positive SCL of the primary streamer is disrupted by negative charge injection from the secondary streamer and electron-ion recombination. As a result, the primary streamer can experience an abrupt change in the direction of propagation, path-deviation, if the disruption alters the SCL's stable, symmetric shape. In these cases, the SCL generally remains contiguous. However, if the secondary streamer is strong enough, the SCL of the primary streamer can be broken into two or more disconnected pieces, each of which can further develop into an individual streamer-streamer branching. In this case, the perturbed SCL is non-contiguous. This sequential process (statistical seeding of electrons by photoionization, avalanche of a secondary streamer, collision with the primary SCL, breaking of the SCL and branching) can consecutively take place at random times and locations. The end result is a multi-level, tree-like plasma channel structure or multi-pronged streamer branching. A number of numerical tests were carried out and nearly identical statistical results were obtained.

In parameterizing the effects of the mean-free-path for photoionizing absorption, we find a trend toward there being fewer, more filamentary branchings as the mean free path for ionization decreases or is more localized near the streamer. With the majority of the photoionization events occurring in closer proximity to the streamer, the likelihood for path-deviation and branching decreases. However, any long mean free path photoionization, as might occur in the wings of the lineshape, appears to be sufficient to provide the stochastic initiating ionizations that could lead to path deviation and branching.

#### Acknowledgments

This work at was supported by the United States Department of Energy Office of Fusion Energy Science (DE-SC0001319) and the National Science Foundation (CHE-1124724).

#### References

- [1] Loeb L B 1939 *Fundamental Processes of Electrical Discharge in Gases* (New York: Wiley)
- [2] Raether H 1939 Die entwicklung der elektronen in den funkenkanal *Z. Angew. Phys.* **112** 464
- [3] Loeb L B and Meek J M 1941 *The Mechanism of the Electric Spark* (Stanford: Stanford University Press)
- [4] van Veldhuizen E M (ed) 2000 *Electrical Discharges for Environmental Purposes: Fundamentals and Applications* (New York: Nova Science)

- [5] Kulikovskiy A A 1988 Positive streamer in a weak field in air: a moving avalanche-to-streamer transition *Phys. Rev. E* **57** 7066
- [6] Briels T M P, Kos J, Winands G J J, van Veldhuizen E M and Ebert U 2008 Positive and negative streamers in ambient air: measuring diameter, velocity and dissipated energy *J. Phys. D: Appl. Phys.* **41** 234004
- [7] Luque A, Ratushnaya V and Ebert U 2008 Positive and negative streamers in ambient air: modelling evolution and velocities *J. Phys. D: Appl. Phys.* **41** 234005
- [8] Vasilyak L M, Kostyuchenko S V, Kudryavtsev N N and Filyugin I V 1994 Fast ionisation waves under electrical breakdown conditions *Phys.—Usp.* **37** 247
- [9] Starikovskaia S M, Anikin N B, Pancheshnyi S V, Zatspein D V and Starikovskii A Yu 2001 Pulsed breakdown at high overvoltage: development, propagation and energy branching *Plasma Sources Sci. Technol.* **10** 344
- [10] Takashima K, Adamovich I V, Xiong Z, Kushner M J, Starikovskaia S, Czarnetzki U and Luggenhölscher D 2011 Experimental and modeling analysis of fast ionization wave discharge propagation in a rectangular geometry *Phys. Plasmas* **18** 083505
- [11] Nijdam S, Moerman J S, Briels T M P, van Veldhuizen E M and Ebert U 2008 Stereo-photography of streamer in air *Appl. Phys. Lett.* **92** 101502
- [12] Ichiki R, Kanazawa S, Tomokiyo K, Hara H, Akamine S, Kocik M and Mizeraczyk J 2011 Observing three-dimensional structures of streamer discharge channels *IEEE Trans. Plasma Sci.* **39** 2228
- [13] Ebert U and Sentman D D 2008 Streamers, sprites, leaders, lightning: from micro- to macroscales *J. Phys. D: Appl. Phys.* **41** 230301
- [14] Hegeler F and Akiyama H 1997 Ozone generation by positive and negative wire-to-plate streamer discharges *Japan. J. Appl. Phys.* **36** 5335
- [15] Samaranyake W J M, Miyahara Y, Namihira T, Katsuki S, Sakugawa T, Hackam R and Akiyama H 2000 Pulsed streamer discharge characteristics of ozone production in dry air *IEEE Trans. Dielectr. Electr. Insul.* **7** 254
- [16] Levatter J I and Lin S C 1980 Necessary conditions for the homogeneous formation of pulsed avalanche discharges at high gas pressures *J. Appl. Phys.* **51** 210
- [17] Brenning N, Axnas I, Nilsson J O and Eninger J E 1997 High-pressure pulsed avalanche discharges: formulas for required pre-ionization density and rate for homogeneity *IEEE Trans. Plasma Sci.* **25** 83
- [18] Dhali S K and Williams P F 1985 Numerical simulation of streamer propagation in nitrogen at atmospheric pressure *Phys. Rev. A* **31** 1219
- [19] Dhali S K and Williams P F 1987 Two-dimensional studies of streamers in gases *J. Appl. Phys.* **62** 4696
- [20] Flegler E and Raether H 1935 Untersuchung von Gasentladungsvorgängen mit der Nebelkammer *Z. Tech. Phys.* **11** 435
- [21] Bradley C D and Snoddy L B 1935 Ion distribution during the initial stages of spark discharge in nonuniform fields *Phys. Rev.* **47** 541
- [22] Zheleznyak M B, Mnatsakanian A K H and Szykh S V 1982 Photoionization of nitrogen and oxygen mixtures by radiation from a gas discharge *High Temp.* **20** 357
- [23] Naidis G V 2006 On photoionization produced by discharges in air *Plasma Sources Sci. Technol.* **15** 253
- [24] Bourdon A, Pasko V P, Liu N Y, Célestin S, Ségur P and Marode E 2007 Efficient models for photoionization produced by non-thermal gas discharges in air based on radiative transfer and Helmholtz equations *Plasma Sources Sci. Technol.* **16** 656
- [25] van Veldhuizen E M and Rutgers W R 2002 Pulsed positive corona streamer propagation and branching *J. Phys. D: Appl. Phys.* **35** 2169
- [26] Ebert U, Montijn C, Briels T M P, Hundsdorfer W, Meulenbroek B, Rocco A and van Veldhuizen E M 2006 The multiscale nature of streamers *Plasma Sources Sci. Technol.* **15** S118
- [27] Takahashi E, Kato S, Sasaki A, Kishimoto Y and Furutani H 2011 Controlling branching in streamer discharge by laser background ionization *J. Phys. D: Appl. Phys.* **44** 075204
- [28] Mesyats G A and Yalandin M I 2009 On the nature of picosecond runaway electron beams in air *IEEE Trans. Plasma Sci.* **37** 785
- [29] Chanrion O and Neubert T 2010 Production of runaway electrons by negative streamer discharges *J. Geophys. Res.* **115** A00E32
- [30] Ebert U *et al* 2011 Multiple scales in streamer discharges, with an emphasis on moving boundary approximations *Nonlinearity* **24** C1
- [31] Luque A and Ebert U 2012 Density models for streamer discharges: beyond cylindrical symmetry and homogeneous media *J. Comput. Phys.* **231** 904
- [32] Li C, Teunissen J, Nool M, Hundsdorfer W and Ebert U 2012 A comparison of 3D particle, fluid and hybrid simulations for negative streamers *Plasma Sources Sci. Technol.* **21** 055019
- [33] Lozansky E D and Firsov O B 1973 Theory of the initial stage of streamer propagation *J. Phys. D: Appl. Phys.* **6** 976
- [34] Arrayas M, Betelu S, Fontelo M A and Trueba J L 2008 Fingering from ionization fronts in plasmas *SIAM J. Appl. Math.* **68** 1122
- [35] Kolobov V I and Arslanbekov R R 2012 Towards adaptive kinetic-fluid simulations of weakly ionized plasmas *J. Comput. Phys.* **231** 839
- [36] Nijdam S, van de Wetering F M J H, Blanc R, van Veldhuizen E M and Ebert U 2010 Probing photo-ionization: experiments on positive streamers in pure gases and mixtures *J. Phys. D: Appl. Phys.* **43** 145204
- [37] Wormeester G, Pancheshnyi S, Luque A, Nijdam S and Ebert U 2010 Probing photo-ionization: simulations of positive streamers in varying N<sub>2</sub>:O<sub>2</sub>-mixtures *J. Phys. D: Appl. Phys.* **43** 505201
- [38] Wormeester G, Nijdam S and Ebert U 2011 Feather-like structures in positive streamers interpreted as electron avalanches *Japan. J. Appl. Phys.* **50** 08JA01
- [39] Luque A and Ebert U 2011 Electron density fluctuation accelerate the branching of positive streamer discharges in air *Phys. Rev. E* **84** 046411
- [40] Pancheshnyi S 2005 Role of electronegative gas admixtures in streamer start, propagation and branching phenomena *Plasma Sources Sci. Technol.* **14** 645–53
- [41] Arrayas M, Baltanas J P and Trueba J L 2008 Fluctuation charge effects in ionization fronts *J. Phys. D: Appl. Phys.* **41** 105204
- [42] Luque A, Ebert U, Montijn C and Hundsdorfer W 2007 Photoionisation in negative streamers: fast computations and two propagation modes *Appl. Phys. Lett.* **90** 081501
- [43] Liu N Y and Pasko V P 2004 Effects of photoionization on propagation and branching of positive and negative streamers in sprites *J. Geophys. Res. (Space Phys.)* **109** A04301
- [44] Vereschagin I P and Beloglavsky A A 2004 Mathematical modeling of pulse streamer corona in air *Proc. 15th Int. Conf. on Gas Discharges and their Applications (Toulouse, France, 2004)* vol 1 p 579
- [45] Xiong Z and Kushner M J 2012 Atmospheric pressure ionization waves propagating through a flexible high aspect ratio capillary channel and impinging upon a target *Plasma Sources Sci. Technol.* **21** 034001

- [46] Xiong Z, Robert E, Sarron V, Pouvesle J-M and Kushner M J 2012 Dynamics of ionization wave splitting and merging of atmospheric-pressure plasmas in branched dielectric tubes and channels *J. Phys. D: Appl. Phys.* **45** 275201
- [47] Wang D, Namihira T and Akiyama H 2011 Propagation of streamer heads during a 5-ns pulsed discharge *IEEE Trans. Plasma Sci.* **39** 2268
- [48] Kulikovskiy A 2000 The role of photoionization in positive streamer dynamics *J. Phys. D: Appl. Phys.* **33** 1514
- [49] Arrayas M, Ebert U and Hundsoerfer W 2002 Spontaneous branching of anode-directed streamers between planar electrodes *Phys. Rev. Lett.* **88** 174502
- [50] Heijmans L C J, Nijdam S, van Veldhuizen E M and Ebert U 2013 Streamers in air splitting into three branches *Europhys. Lett.* **103** 25002
- [51] Uddi M, Jiang N, Adamovich I V and Lempert W R 2009 Nitric oxide density measurements in air and air/fuel nanosecond pulse discharges by laser induced fluorescence *J. Phys. D: Appl. Phys.* **42** 075205